Current Research in Microbial Sciences 3 (2022) 100164

Contents lists available at ScienceDirect

Current Research in Microbial Sciences

journal homepage: www.sciencedirect.com/journal/current-research-in-microbial-sciences

Modeling the elemental stoichiometry and silicon accumulation in diatoms

Gabrielle Armin *, Keisuke Inomura

Graduate School of Oceanography, University of Rhode Island, Narragansett, RI , United States

ARTICLE INFO

Keywords:
Quantitative model
Nutrients
Macromolecules
Proteins
Biosynthesis
Metabolism
Phytoplankton
Silica
Silicon

ABSTRACT

Diatoms are important microorganisms involved in global primary production, nutrient cycling, and carbon sequestration. A unique feature of diatoms is their silica frustules, which impact sinking speed, defense against predators and viruses, and growth cycling. Thus, frustules are inherently linked to their role in ecosystems and biogeochemical cycles. However, constraints on cellular silicon levels remain unclear and few existing models resolve diatom elemental stoichiometry to specifically include variable silicon levels. Here, we use a coarse-grained model of the diatom, Thalassiosira pseudonana, compared with laboratory results to illustrate the relationship of silicon uptake with elemental stoichiometry of other nutrients. The model-data comparison suggests the balance between growth rate and silicon uptake constrains the amount of cellular silicon. Additionally, it expresses relationships between silicon, nitrogen, phosphorus, and carbon to changing growth rates in nitrogen-limited and phosphorus-limited regimes. First, our model-data comparison suggests Si uptake hits a maximum cellular quota at low growth rates and below this maximum there is independent Si uptake. In each nutrient regime, Si:N, Si:P, and Si:C decrease exponentially with growth rate when Si is below the maximum limit. This is explained by independent Si uptake and increased loss of Si to new cells. These results provide predictions of diatom stoichiometry and allocation, which can be used in ecosystem models to differentiate phytoplankton types to better represent diatoms' contribution to global biogeochemical cycles and ecosystems.

1. Introduction

Diatoms are a major group of eukaryotic phytoplankton whose cells are encompassed in a silica frustule (shell-like structure). These organisms are essential in biogeochemical cycles drawing carbon dioxide from their surroundings for photosynthesis, sequestering carbon by export to the deep oceans (Michaels and Silver, 1988; Legendre and Le Fevre, 1995; Richardson and Jackson, 2007), and providing a large fraction of the world's primary production (Field et al., 1998). Accurately modelling their important role in biogeochemical cycles and primary production is thus inherently linked with resolving silica constraints. While diatoms are significant players in the carbon (C) and silicon (Si) cycles, they also have a large effect on other major nutrient cycles including nitrogen (N) and phosphorus (P) cycles (Broecker, 1982; Yvon-Durocher et al., 2015). Diatoms use N and P to perform essential cellular tasks, such as photosynthesis, biosynthesis and glycolysis, which provide the cell with energy and contribute to growth (Wheeler, 1983; Brown et al., 2004), while Si is used to build frustules to defend from predators (Hamm et al., 2003) and viruses (Kranzler et al., 2019) and to modulate their buoyancy (Smetacek, 1985; De Tommasi et al., 2017). Specifically, the amount of Si incorporated into the frustule affects their sinking velocity (Anderson and Sweeney, 1978; Waite et al., 1997), which allows them to regulate their position in the water column. Diatoms adjust their buoyancy in response to irradiance (Bienfang et al., 1983) and nutrient concentration (Bienfang et al., 1982), suggesting regulation of their position in the water column is dependent on energy (Waite et al., 1992) and necessary for cell survival (Behrenfeld et al., 2021). Thicker layers of Si in the frustule enhance sinking, increasing the probability that the carbon will be sequestered in the deep (Finkel et al., 2005). Conversely, if a diatom frustule has lower concentrations of Si, there is a greater potential the carbon will be remineralized in the surface ocean and remain active in the carbon cycle (Tréguer et al., 2018).

Elemental ratios (i.e. stoichiometry) of these nutrients describe the nutrient availability in the surface and deep ocean, point to the potential for sinking and export (Broecker, 1982), and indicate the nutritional value of diatoms for higher trophic organisms (Finkel et al., 2016; Makareviciute-Fichtner et al., 2021; Duncan et al., 2022). For these reasons, it is important to quantify cellular elemental stoichiometry of diatoms to understand their role in global biogeochemical cycles and marine ecosystems. Furthermore, it is necessary to quantify intracellular

* Corresponding author.
E-mail address: garmin@uri.edu (G. Armin).

https://doi.org/10.1016/j.crmicr.2022.100164

Available online 20 September 2022

nutrient interactions to determine how environmental conditions, specifically nutrient regimes, alter cellular elemental stoichiometry. Currently, there are outstanding questions about whether the uptake of Si is related to the uptake of other nutrients (N and P). The rate of Si-uptake is believed to be only a function of the bioavailable extracellular Si (Thamatrakoln and Hildebrand, 2008) and the stage of cellular division (Brzezinski et al., 1990; Bowler et al., 2010). Generally, Si uptake follows the Michaelis-Menten formulation of saturating nutrient uptake and is observed across taxa within diatoms (Paasche, 1973).

Although laboratory studies observe uptake interactions between nutrients in diatoms (Tilman and Kilham, 1976; Lomas and Glibert, 2000; Lynn et al., 2000; Claquin et al., 2002; Spilling et al., 2015), current models resolving the interaction between Si and other nutrients tend to lack explicit comparison between the model results and empirical data (Flynn, 2001) or are on the genomic-scale, which is highly specific (Van Tol et al., 2021). Other existing models analyze a diatom's intracellular reactions such as C allocation and C exchange in diatoms (Smith and Geider, 1985) or predict the diatom size and shape over the entirety of the cell cycle (Hicks et al., 2006). Additionally, there are models to resolve complex interactions in the Si frustule such as characterizations of porous layers in the frustule (Lu et al., 2015), size effects of nanoporous Si (Sen et al., 2011), and mechanical properties of the frustule (Topal et al., 2020). However, these models do not couple the nutrients used intracellularly (N, P, and C) and the accumulation of Si in the frustule. Including this nutrient in diatom cell models before incorporating them into large biogeochemical models is an integral step in creating accurate global models especially due to that fact that diatoms have a significant impact on the global Si cycle accounting for 240 Tmol of biogenic Si precipitation annually (Falkowski and Raven, 2013). Not only this, but these interactions could differentiate diatoms from other groups of phytoplankton. Since nutrient constraint by various phytoplankton types is currently unresolved, many ecosystem models that include lower trophic organisms rely on a simple separation between phytoplankton types often based on their size class (Dunne et al., 2005; Zahariev et al., 2008; Watanabe et al., 2011). However, there is likely a discrepancy in nutrient uptake between diatoms and other groups of phytoplankton because many other taxa do not accumulate cellular Si nor have a Si frustule, which could affect nutrient accumulation due to decreased surface areas where active nutrient uptake can occur (Finkel and Kotrc, 2010). Previously, an experimentalist called for more mechanistic models of diatoms that can be used to evaluate the relationship between nutrients that could also be used to differentiate phytoplankton functional groups (Gilpin et al., 2004). Mechanistic models, specifically coarse-grained models, offer a unique opportunity to represent these interactions within a diatom as they often represent complex, cellular systems effectively by lowering resolution of the interactions from the atomic level to macromolecules (Ingólfsson et al., 2014; Kmiecik et al., 2016).

Here, we present a simple, mechanistic model of nutrient uptake, elemental stoichiometry, and allocation which we compared to observational data (Claquin et al., 2002) from cultures of the marine diatom, *Thalassiosira pseudonana*, to address the following questions. [1] How does a diatom allocate nutrients to macromolecular pools with increasing growth rate? [2] How does the Si accumulation change with varying growth rate and nutrient regimes? [3] How is the intracellular level of Si constrained relative to other nutrients (C/N/P)?

2. Methods

Our cellular diatom model (Cell Flux Model of Si accumulation: CFM-Si) (Fig. 1) predicts steady-state uptake and allocation of nutrients (Si, N, P, C) as well as the resulting elemental stoichiometry with varying growth rates under two nutrient regimes, N-limited and P-limited. Here, the difference between N-limited and P-limited regimes is the addition of N storage in a P-limited environment due to the excess N availability, and similarly, P storage in a N-limited environment. We compared our model results to laboratory data (Claquin et al., 2002) from continuous cultures of the diatom species *Thalassiosira pseudonana* grown in artificial seawater F/2 medium in both N and P-limited laboratory conditions at a constant irradiance, cell density, and temperature (I =150 μmol photons m^{-2} s^{-1}, T = 19 °C). *Thalassiosira pseudonana* is considered an average-sized (Kipp et al., 2019), centric diatom known to both form chains of cells (Waite et al., 1997; Davis et al., 2005; Hildebrand et al., 2007) or remain as a single-celled organism. Species of the genus *Thalassiosira* are found in many regions of the ocean including coastal and open ocean regions, as well as in estuarine systems (Pratt, 1965; Aizawa et al., 2005; Hoppenrath et al., 2007; Yoshie et al., 2010; Leblanc et al., 2012; Rynearson et al., 2020). Since the sequencing of its genome, *Thalassiosira pseudonana* has served as a model organism for the general group of diatoms (Armbrust et al., 2004; Parker et al., 2008). Along with these constraints from laboratory data, our model uses mathematical representations of cellular processes.

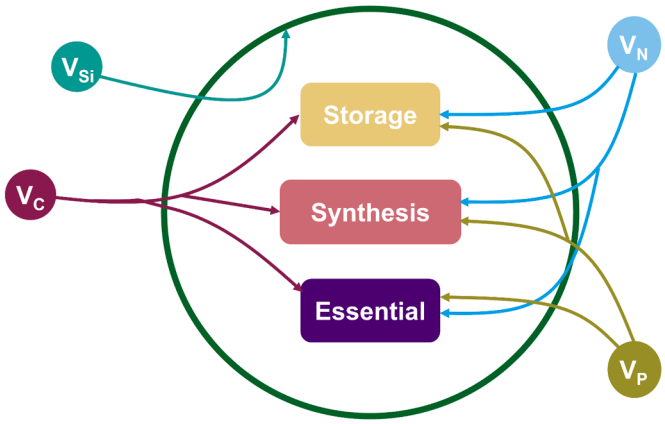

Fig. 1. Schematic of elemental uptake and allocation model with Si: CFM-Si. The cell uptakes C (V_C: maroon circle), N (V_N: blue circle), and P (V_P: olive circle) and allocates (indicated by the maroon, blue, and olive arrows corresponding to respective nutrient) them to different macromolecular pools (rounded, color-coded rectangles): storage (yellow), synthesis (pink), and essential (purple) macromolecules. Synthesis encompass all proteins associated with photosynthesis and biosynthesis as well as RNA. Within the synthesis pool there are essential proteins that remain constant through model runs. Essential macromolecules are assumed constant and include DNA, RNA, and structural components such as lipids in the cellular membrane. C storage includes carbohydrates and lipids. We assumed polyphosphate molecules comprise P storage and N storage is made up of proteins. Storage only occurs when the respective nutrient is not limited. The cell also uptakes Si (V_{Si}: teal circle), which is directly allocated (teal arrow) to the silica frustule/cell wall.

2.1. Si accumulation

To obtain the concentration of Si (pmol Si $cell^{-1}$) we divided Si accumulation rate (V_{Si}) per cell (pmol Si $cell^{-1}$ d^{-1}) by the growth rate (μ) (d^{-1}).

$$Si = \frac{V_{Si}}{\mu} \quad (1)$$

Here, we assumed Si-replete conditions and that all Si in the cell is directly allocated to the cell wall, specifically the frustule. This equation represents the balance between uptake of Si and cost of Si to make new cells. For example, if the growth rate is large, the cell accumulates a smaller amount of Si because a majority of the Si goes towards building new cells. A large growth rate also creates a small time frame for the cell to accumulate Si since new cells are made quickly. We chose to parameterize our model using V_{Si} = 0.14 (pmol Si $cell^{-1}$ d^{-1}) for both the N-limited and P-limited cases, which is within the observed range (Paasche, 1973) for the diatom *Thalassiosira pseudonana*. We chose this value when parameterizing our model to best represent the data.

Additionally, we imposed a maximum Si quota, 0.96 pmol Si cell^{-1} for both the N-limited and P-limited environments, to align with an observed maximum Si value (Claquin et al., 2002). Although we used one species of diatom within our model, the equation can be parameterized for numerous species using different values for V_{Si} obtained through laboratory studies (Paasche, 1973; Martin-Jézéquel et al., 2000).

2.2. Si related elemental stoichiometry

Due to the conservation of mass, the elemental stoichiometry in the cell is the result of the uptake of different elements. Therefore, the elemental ratios of Si:C, Si:N, and Si:P, are obtained by the following equations:

$$Si : C = V_{Si} : V_C \tag{2}$$

$$Si : N = V_{Si} : V_N \tag{3}$$

$$Si : P = V_{Si} : V_P \tag{4}$$

Here, V_C (pmol C cell^{-1} d^{-1}), V_N (pmol N cell^{-1} d^{-1}), and V_P (pmol P cell^{-1} d^{-1}) denote the uptake rate of C, N and P per cell. We wish to point out, due to the lack of empirical observation, our results involving P are model predictions. Additionally, we used least-squares regression to compare our model results with the data provided by Claquin et al. (2002) and to evaluate the strength of our model's predictions.

2.3. Uptake of N, P and C

As stated in the previous section, the key to obtaining Si:C, Si:N and Si:P are the uptake rates. First, to obtain the uptake rate of C (V_c) (pmol C cell^{-1} d^{-1}), we use a relationship between the amount of C-based biomass (Q_c) (pmol C cell^{-1}) and growth rate (μ) based on the mass conservation where uptake is balanced by the biomass synthesis:

$$V_c = \mu Q_c \tag{5}$$

We estimated Q_c based on the linear regression of Q_c-μ relationship in Claquin et al. (2002). Similarly to V_c, V_N and V_P are related to the growth rate based on the mass balances:

$$V_N = \mu Q_c \times N : C \tag{6}$$

$$V_P = \mu Q_c \times P : C \tag{7}$$

where N:C and P:C are the stoichiometric ratios of cellular N to C (mol N mol C^{-1}) and P to C (mol P mol C^{-1}).

2.4. Macromolecular allocations

To obtain N:C and P:C, the model considers macromolecular allocation under different conditions. Our model allocates N, P, and C to three similar macromolecular pools: essential, photosynthetic and biosynthetic macromolecules grouped into a pool termed "Synthesis", and storage for N, P and C (Fig. 1). The formulation of equations are adapted from a previously published macromolecular model of phytoplankton (Inomura et al., 2020). The storage pool varies among nutrients; C storage is comprised of lipids and carbohydrates, while N storage is protein, and polyphosphates comprise P storage. Essential proteins remain constant throughout the simulations. C and P allocation have the additional macromolecular pool "essential", which refers to the C-rich macromolecules as well as the minimum level of P-rich RNA molecules necessary for basic cell structure and cell survival. We quantified these macromolecular pools alone for simplicity, using the assumption that proteins often account for a large fraction of the amount of C and N in the cell (Anderson, 1995; Geider and La Roche, 2002).

Our first macromolecular allocation representation Eq. (4) demonstrates the allocation of N to three pools,

$$N : C = Pro_{essential} + \mu Pro_{synth} + N_{sto} \tag{8}$$

where Pro_{synth} is the rate of protein synthesis for proteins associated with photosynthesis and biosynthesis (mol N mol C^{-1} d) (Inomura et al., 2019, 2020), and N_{sto} is the proportion of nutrients dedicated to N storage within the cell (mol N mol C^{-1}). This formula is based on the assumption that proteins and N storage account for a large percent of the N and C found within a cell (Anderson, 1995; Geider and La Roche, 2002; Inomura et al., 2020). The linear relationship of synthetic protein to the growth rate is consistent with prior observations of linearly increasing investment to ribosomal proteins and protein-based N with growth rate (Rhee, 1978; Jahn et al., 2018; Zavřel et al., 2019). We set the value for Pro_{synth} to be 0.1 mol N mol C^{-1} d, which is in a reasonable range consistent with previous studies (Inomura et al., 2020; Armin and Inomura, 2021). N storage only occurs when N is in excess, therefore the N-limited simulation does not include N storage. We chose a constant value of 0.035 mol N mol C^{-1} for N storage as it aligns with previous modeling work (Inomura et al., 2020). $Pro_{essential}$ is the stoichiometric ratio of essential proteins (mol N mol C^{-1}), which remains constant through simulations, set at 0.03, seen in the data in which we compare our model results (Claquin et al., 2002). We assumed essential proteins to consist of those not directly involved in biosynthesis or photosynthesis, for example transmembrane proteins.

Next, we separated P into three macromolecular pools Eq. (9),

$$P : C = P : C_{min} + RNA + P_{sto} \tag{9}$$

where $P : C$ is the stoichiometric ratio of P to C (mol P mol C^{-1}), $P : C_{min}$ is the minimum value of P:C (7.2×10^{-4} mol P mol C^{-1}), largely represented by essential P within the cell such as phospholipids. RNA represents the varying amount of RNA in the cell (mol P mol C^{-1}), which is in charge of protein synthesis, and P_{sto} is the amount of P dedicated to storage as polyphosphates (mol P mol C^{-1}). We calculated RNA Eq. (10) by multiplying the amount of protein proxied by N:C (mol N mol C^{-1}) by the growth rate, μ (d^{-1}), a constant x_{RNA} (1.9×10^{-2} mol P d mol N^{-1}) (Inomura et al., 2020).

$$RNA = N : C \times \mu \times x_{RNA} \tag{10}$$

This formula is based on the observation of the linear relationship between RNA and protein and growth rate (Nicklisch and Steinberg, 2009; Scott et al., 2010; Inomura et al., 2020). When P is not limited, the excess P can be accumulated, which is commonly observed behavior of diatoms (Raven, 1997; Tozzi et al., 2004). We quantified P_{Sto} by using the following relationship Eq. (11),

$$P_{sto} = \frac{Q_P^{max}}{Q_c} - P : C_{min} - RNA \tag{11}$$

where Q_P^{max} is the maximum amount of P in the cell (pmol P cell^{-1}) Eq. (12). To obtain Q_P^{max}, we used the total amount of C (pmol C cell^{-1}) divided by a commonly observed C:P = 65 (mol C mol P^{-1}) under P replete conditions (Quigg et al., 2003; King et al., 2015) in diatoms to obtain a maximum value of Q_P.

$$Q_P^{max} = \frac{Q_C}{65} \tag{12}$$

We then used the ratios of P:C and N:C to predict the elemental stoichiometry of N:P using Eq. (13) and included these results in the supplemental material.

$$N : P = \frac{N : C}{P : C} \tag{13}$$

Lastly, we separated C into four macromolecular pools,

$$C_{allocation} = C_{essential} + C : N_{pro}\left(Pro_{essential} + \mu Pro_{synth}\right) + C_{sto} \tag{14}$$

where $C_{essential}$ is the fraction of C (mol C mol C^{-1}) allocated to essential macromolecules for cell survival (here we exclude proteins to avoid double counting), $C:N_{pro}$ is the molar ratio of C to N in proteins (mol C mol N^{-1}), and C_{sto} is C storage within the cell (mol C mol N^{-1}). For C allocation, it is important to note C_{sto} and $C_{essential}$ are not represented by proteins, but other macromolecules including carbohydrates and lipids within storage and DNA and lipids within $C_{essential}$. We expressed C allocation as a percentage to get an overall picture of the cell's dedication to varying cellular processes. This formulation assumes that the contribution from RNA is small, as predicted in a previous model (Inomura et al., 2020).

3. Results and discussion

3.1. Uptake of Si

In each modeled nutrient regime (Fig. 2), there is high cellular concentrations of Si at low growth rates. The uptake of Si into the frustule is a thermodynamically favorable process (Martin-Jézéquel et al., 2000; De Tommasi et al., 2017), meaning the cell uses little energy when accumulating Si into the frustule. There is maximum Si accumulation at low growth rates when most of the energy is dedicated to the creation of the cell wall, suggesting the process of incorporating Si coincides with the cell cycle. Mathematically, given the uptake of Si is independent of other metabolisms (Thamatrakoln and Hildebrand, 2008), as the growth rate increases the cell allocates more Si to build new cells, which accounts for the decreasing Si accumulation per cell. This trend is largely supported by the data (Fig. 2) and validates earlier experimental research suggesting mineralization is inversely correlated to growth rate (Martin-Jézéquel et al., 2000). In several species, mineralization occurs for the duration of cell wall synthesis to enhance the creation of new valves (Brzezinski et al., 1990; Martin-Jézéquel et al., 2000). Additionally, there is a limit to the amount of Si the cell can accumulate at low growth rates, therefore we imposed a maximum value (Fig. 2c). If this maximum were not imposed, the Si content would approach infinity when the growth rate is very low, which is not the case in nature and observations. As the growth rate starts to increase, the Si content per cell eventually starts to decline exponentially.

3.2. Macromolecular allocation of N and C

Under N-limitation, a higher proportion of N is allocated to proteins as the growth rate increases (Fig. 3A). The essential proteins stay at a constant ratio of 0.03 mol N mol C^{-1}, while the synthetic proteins increase linearly from 0.03 to 0.13 mol N mol C^{-1}. In this nutrient regime, there is no allocation of N to N storage because N is limiting. However, there is allocation of P to P storage due to luxury uptake (Fig. 3B). P storage depletes with growth rate as the dedication to synthesis molecules increases, specifically to RNA. Here, since there is excess P, the slowing of protein production, due to the lack of N, must cause the dedication of P to RNA to cease. In a similar manner, C storage (Fig. 3C), decreases with increasing growth rate from 45% of the intracellular C at a growth rate of 0 to approximately 0% of the intracellular C at a growth rate of 1.0 d^{-1}. At low growth rates, this fraction of C allocated to storage can be used as energy for cellular processes such as cellular respiration. The proportion of C dedicated to synthetic proteins acts inversely, increasing from 0 to 45% with growth rate. There is an additional dedication to the essential proteins that remains constant with growth rate comprising 13% of total C. At low growth rates, catalyzing important cellular reactions requires less protein due to the slower pace at which the new cells are produced. However, as cells grow faster, more synthetic proteins are needed to produce new cells at a higher rate.

Generally, under P-limitation, the macromolecular pool of synthetic molecules is increasing with growth rate. The proportion of N (Fig. 3D) dedicated to synthetic proteins increases linearly by 0.09 mol N mol C^{-1}, while the fraction of P (Fig. 3E) increases exponentially from 7.2×10^{-4} to 3.82×10^{-3} mol P mol C^{-1}. The major difference between the two nutrient regimes is the dedication of N to storage instead of P. When P is limited, RNA production is also limited, which will eventually limit protein synthesis. This explains why N storage remains constant with growth rate and N allocation to synthetic proteins only increases by a factor of 2.5 rather than a factor of 4.2 seen in N-limitation. The fraction of C allocated to various macromolecular pools (Fig. 3C, F) does not vary between nutrient regimes, and thus growth rate is the main factor that dictates macromolecular allocation of C. Eventually, we may consider multiple species of N and P in allocation for various nutrient regimes because this could impact not only the N or P concentrations directly, but also the C content in the cell. For example, it takes less energy for the cell to use ammonium in the cell compared to nitrate (Thauer et al., 1977; Strohm et al., 2007) so the loss of C, used in energy production, is reduced, which may lead to an overall decrease in N:C.

3.3. Elemental stoichiometry

For both nutrient scenarios, N:C increases linearly with growth rate, represented strongly by the model under both N-limitation (Fig. 4A) (R^2=0.999) and P-limitation (Fig. 4E) (R^2=0.999). Additionally, the nutrient ratios for Si:N (Fig. 4B, F), Si:C (Fig. 4C, G), and Si:P (Fig. 4D, H) all exponentially decrease with growth rate for both nutrient regimes when Si per cell is below the maximum limit. The slope is milder when Si reaches the maximum amount (at lower growth rate), because of the constant Si per cell. On top of this, the other nutrients vary between the two nutrient regimes. Si:N and Si:P vary due to the existence of storage

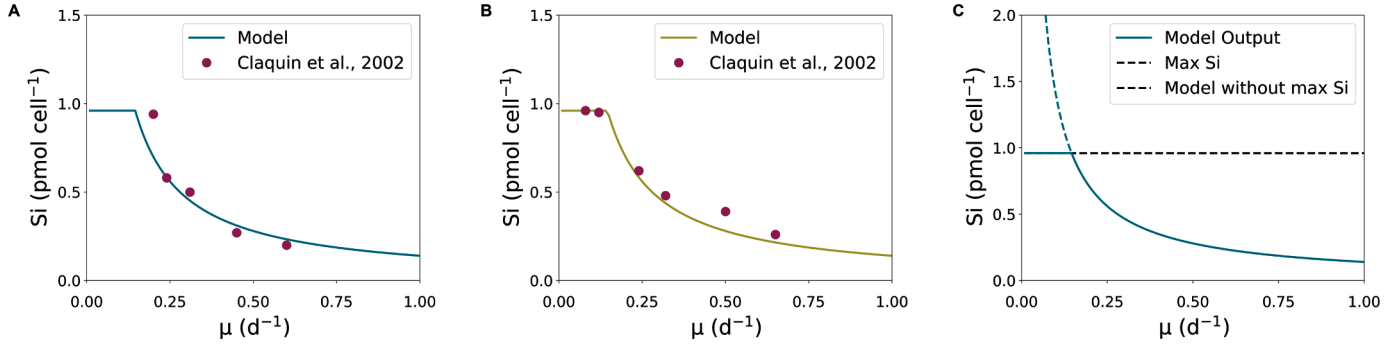

Fig. 2. Observations and modeled concentration (pmol Si $cell^{-1}$) of Si for N-limited regimes (A) and P-limited regimes (B). N-limited model lines are represented by teal lines, while the olive lines represent the P-limited model. We compare the modeled (solid lines) Si concentration for increasing growth rate (A, B) to Claquin et al. (2002) culture data (circles). Schematic (C) demonstrating the model without an imposed maximum (teal, dashed line), the value of the maximum Si content, and the model with a maximum Si content per cell (teal, solid line) for increasing growth rate.

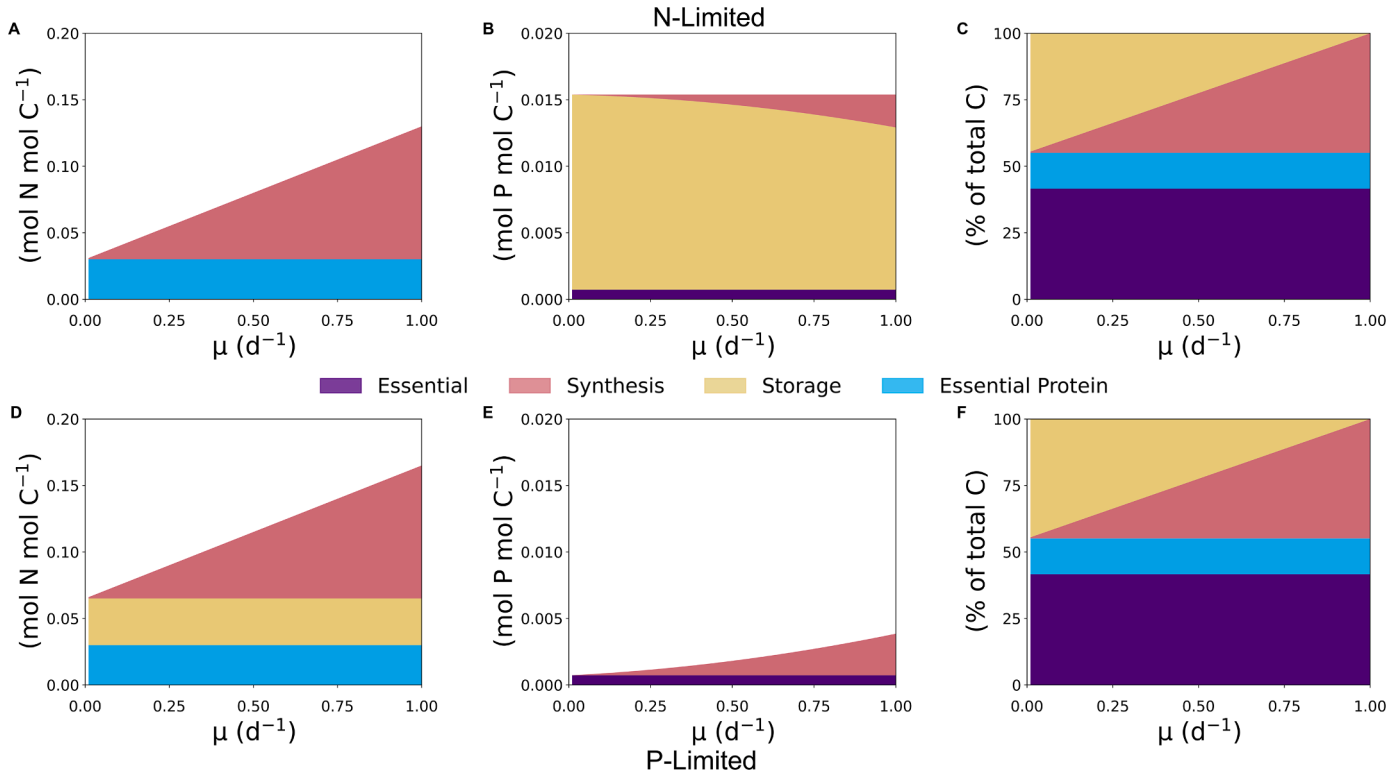

Fig. 3. N:C allocation (mol N mol C^{-1}), P:C allocation (mol P mol C^{-1}), and C allocation to macromolecular pools including essential molecules (purple), biosynthesis (pink), minimum protein (blue) and storage (yellow) for increasing growth rate in an N-limited nutrient scenario (A, B, C) and a P-limited nutrient scenario (D, E, F).

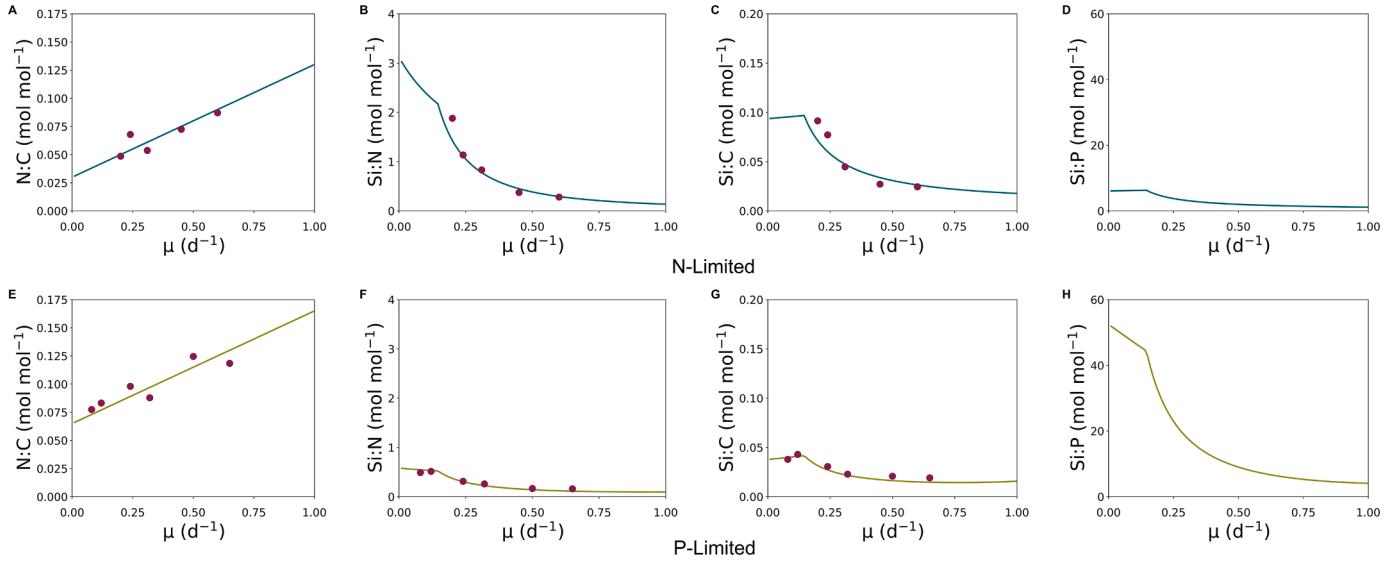

Fig. 4. Modeled elemental ratios (solid lines) of N:C (A, E), Si:N (B, F), Si:C (C, G), and Si:P (D, H) with increasing growth rate in a N-limited nutrient regime (teal lines) and a P-limited regime (olive lines). Here, we compare model results to culture data (maroon circles) from Claquin et al. (2002). Elemental ratios are measured in mole/mole of the respective nutrient (i.e. mol N mol C^{-1}).

when the respective nutrients are not limited. Additionally, the lower Si:C values at lower growth rates when P is limited correspond to previous laboratory studies that observed increasing absolute C under P limitation (Obata et al., 2013; Brembu et al., 2017; Panagiotopoulos et al., 2020). Lastly, there is large variation between the two modeled nutrient regimes in N:P (Fig. S1). Under N-limitation, N:P increases linearly with increasing growth rate because of the linear increase in N:C and a constant P:C value due to P storage. Conversely, N:P decreases in a P-limited regime because N still increases linearly while P increases exponentially. Note the difference in magnitude between the two nutrient scenarios due to the excess of P with N-limitation and lack of P under P-limitation. The variation in nutrient ratios with growth rate is largely explained by macromolecular allocation. As growth rate increases, the demand for N-rich proteins increases, thus the focus of cellular tasks shifts from constructing the Si frustule to growing faster or larger. Before cell division, the amount of intracellular N, P and C is high, but Si is low in order to facilitate separation into daughter cells.

These elemental ratios may hint to larger processes that govern

ecosystem health and global biogeochemical cycles including nutritional quality for higher trophic levels and C export and sequestration. Understanding the relationship between nutrients allows us to evaluate how abiotic changes to an ecosystem may affect diatom physiology, which in turn affects the overall health of the ecosystem. Specifically, diatoms provide higher trophic levels with lipids used for energy (Hagen and Auel, 2001), proteins for building amino acids (Ruess and Müller-Navarra, 2019) and contributing to overall cellular N (Finkel et al., 2016). Moreover, lower Si:N ratios may point to more favorable nutritional quality for a copepod diet (Makareviciute-Fichtner et al., 2021). The elemental ratios also point to a connection between the amount of C exported to the deep ocean and the concentration of Si in the diatom cell. Thicker, larger Si frustules enhance sinking, and our model illustrates high C storage when Si uptake and concentration is high, suggesting a higher likelihood of deposition C in the deep ocean. However, the concentration of C at this stage is lower compared to higher growth rates. The elemental stoichiometric ratios of Si:N and Si:C indicate that faster growth rates, usually associated with larger diatoms, incorporate more N and C for essential cell processes such as photosynthesis and biosynthesis. In this case, a larger diatom does not necessarily mean it is denser, so the potential for C export may not increase with growth rate. Ultimately, our hope is to incorporate our model framework into larger ecosystem and biogeochemical models to improve our understanding of diatoms' role in global cycles.

5. Conclusion

This study's results illustrate the intracellular level of Si is constrained by growth rate and maximum cellular Si. Our model is unique as it is supported by empirical data and provides predictions of macromolecular allocation alongside elemental stoichiometry in diatoms. Moreover, we predicted the role of P in elemental ratios and macromolecular allocation, which can lead to future experimental work to compare observational data to our model results. The uptake and use of Si in diatom frustules is inherently connected to their role in biogeochemical cycles and modeling these interactions between nutrients in diatoms is essential to better represent their role in biogeochemical cycling. In this study, we offer a framework that may be the next step towards creating large ocean models with representation of many phytoplankton types which can improve the output of existing biogeochemical models. Diatom's unique physiology should be distinguished from other phytoplankton groups to represent the lower trophic level's contribution to the larger ecosystem more accurately. Not only this, resolving this aspect in large biogeochemical models may lead to quantifying the fraction of C deposited into the deep ocean by diatoms specifically or predicting major changes to the food web due to diatom physiology.

Statement of competing interest

The authors declare that they have no known competing financial interests or personal relationships that could have appeared to influence the work reported in this paper.

CRediT authorship contribution statement

Gabrielle Armin: Methodology, Software, Visualization, Formal analysis, Investigation, Writing – original draft, Writing – review & editing. **Keisuke Inomura:** Conceptualization, Methodology, Software, Writing – review & editing, Supervision, Funding acquisition.

Declaration of Competing Interest

The authors declare that there is no conflict of interest.

Model Availability

The model code for this study can be found in (https://zenodo.org/badge/latestdoi/440678631).

Acknowledgments

This material is based upon work supported in part by the National Science Foundation under EPSCoR Cooperative Agreement #OIA-1655221. We thank Katherine Roche, Somang Song, and Virginie Sonnet for helpful discussion on overall clarity and structure of the paper. Additionally, we would like to extend gratitude to Dr. Colleen Mouw for her insightful advice on scientific writing. We also thank Heather McNair for useful discussion on diatoms.

Supplementary materials

Supplementary material associated with this article can be found, in the online version, at doi:10.1016/j.crmicr.2022.100164.

References

Aizawa, C., Tanimoto, M., Jordan, R.W, 2005. Living diatom assemblages from North Pacific and Bering Sea surface waters during summer 1999. Deep. Res. Part II Top. Stud. Oceanogr. 52, 2186–2205. https://doi.org/10.1016/j.dsr2.2005.08.008.

Anderson, L.A., 1995. On the hydrogen and oxygen content of marine phytoplankton. Deep. Res. Part I 42, 1675–1680. https://doi.org/10.1016/0967-0637(95)00072-E.

Anderson, L.W.J., Sweeney, B.M., 1978. Role of inorganic ions in controlling sedimentation rate of marine centric diatom *Ditylum brightwelli*. J. Phycol.

Armbrust, E.V., Berges, J.A., Bowler, C., Green, B.R., Martinez, D., Putnam, N.H., et al., 2004. The genome of the diatom *Thalassiosira pseudonana*: ecology, evolution, and metabolism. Science 306, 79–86. https://doi.org/10.1126/science.1101156.

Armin, G., Inomura, K., 2021. Modeled temperature dependencies of macromolecular allocation and elemental stoichiometry in phytoplankton. Comput. Struct. Biotechnol. J 19, 5421–5427.

Behrenfeld, M.J., Halsey, K.H., Boss, E., Karp-Boss, L., Milligan, A.J., Peers, G., 2021. Thoughts on the evolution and ecological niche of diatoms. Ecol. Monogr. 91, 1–25. https://doi.org/10.1002/ecm.1457.

Bienfang, P.K., Harrison, P.J., Quarmby, L.M., 1982. Sinking rate response to depletion of nitrate, phosphate and silicate in four marine diatoms. Mar. Biol. 67, 295–302. https://doi.org/10.1007/BF00397670.

Bienfang, P., Szyper, J., Laws, E., 1983. Sinking rate and pigment responses to light-limitation of a marine diatom - implications to dynamics of chlorophyll maximum layers. Oceanol. Acta 6, 55–62.

Bowler, C., De Martino, A., Falciatore, A., 2010. Diatom cell division in an environmental context. Curr. Opin. Plant Biol. 13, 623–630. https://doi.org/10.1016/j.pbi.2010.09.014.

Brembu, T., Mühlroth, A., Alipanah, L., Bones, A.M., 2017. The effects of phosphorus limitation on carbon metabolism in diatoms. Philos. Trans. R. Soc. B Biol. Sci. 372 https://doi.org/10.1098/rstb.2016.0406.

Broecker, W. S. (1982). Ocean chemistry during glacial time. 46, 1689–1705.

Brown, J.H., Gillooly, J.F., Allen, A.P., Savage, V.M., West, G.B., 2004. Toward a metabolic theory of ecology. Ecology 85, 1771–1789. https://doi.org/10.1007/978-3-030-64130-6_8.

Brzezinski, M., Olson, R., Chisholm, S., 1990. Silicon availability and cell-cycle progression in marine diatoms. Mar. Ecol. Prog. Ser. 67, 83–96. https://doi.org/10.3354/meps067083.

Claquin, P., Martin-Jézéquel, V., Kromkamp, J.C., Veldhuis, M.J.W., Kraay, G.W., 2002. Uncoupling of silicon compared with carbon and nitrogen metabolisms and the role of the cell cycle in continuous cultures of *Thalassiosira pseudonana* (Bacillariophyceae) under light, nitrogen, and phosphorus control. J. Phycol. 38, 922–930. https://doi.org/10.1046/j.1529-8817.2002.t01-1-01220.x.

Davis, A.K., Hildebrand, M., Palenik, B., 2005. A stress-induced protein associated with the girdle band region of the diatom *Thalassiosira pseudonana* (Bacillariophyta). J. Phycol. 41, 577–589. https://doi.org/10.1111/j.1529-8817.2005.00076.x.

De Tommasi, E., Gielis, J., Rogato, A., 2017. Diatom frustule morphogenesis and function: a multidisciplinary survey. Mar. Genom. 35, 1–18. https://doi.org/10.1016/j.margen.2017.07.001.

Duncan, R.J., Nielsen, D.A., Sheehan, C.E., Deppeler, S., Hancock, A.M., Schulz, K.G., et al., 2022. Ocean acidification alters the nutritional value of Antarctic diatoms. New Phytol. 233, 1813–1827. https://doi.org/10.1111/nph.17868.

Dunne, J.P., Armstrong, R.A., Gnnadesikan, A., Sarmiento, J.L., 2005. Empirical and mechanistic models for the particle export ratio. Glob. Biogeochem. Cycles 19, 1–16. https://doi.org/10.1029/2004GB002390.

Falkowski, P.G., Raven, J.A, 2013. Aquatic Photosynthesis, 2nd ed. Princeton University Press, Princeton, NJ. https://doi.org/10.1515/9781400849727. Available at:

Field, C.B., Behrenfeld, M.J., Randerson, J.T., Falkowski, P., 1998. Primary production of the biosphere: integrating terrestrial and oceanic components. Science 281, 237–240. https://doi.org/10.1126/science.281.5374.237.
Finkel, Z.V., Follows, M.J., Liefer, J.D., Brown, C.M., Benner, I., Irwin, A.J., 2016. Phylogenetic diversity in the macromolecular composition of microalgae. PLoS One 11, 1–16. https://doi.org/10.1371/journal.pone.0155977.
Finkel, Z.V., Katz, M.E., Wright, J.D., Schofield, O.M.E., Falkowski, P.G., 2005. Climatically driven macroevolutionary patterns in the size of marine diatoms over the Cenozoic. Proc. Natl. Acad. Sci. U. S. A. 102, 8927–8932. https://doi.org/10.1073/pnas.0409907102.
Finkel, Z.V., Kotrc, B., 2010. Silica use through time: Macroevolutionary change in the morphology of the diatom fustule. Geomicrobiol. J. 27, 596–608. https://doi.org/10.1080/01490451003702941.
Flynn, K.J., 2001. A mechanistic model for describing dynamic multi-nutrient, light, temperature interactions in phytoplankton. J. Plankton Res. 23, 977–997.
Geider, R.J., La Roche, J., 2002. Redfield revisited: variability of C:N:P in marine microalgae and its biochemical basis. Eur. J. Phycol. 37, 1–17. https://doi.org/10.1017/S0967026201003456.
Gilpin, L.C., Davidson, K., Roberts, E., 2004. The influence of changes in nitrogen: silicon ratios on diatom growth dynamics. J. Sea Res. 51, 21–35. https://doi.org/10.1016/j.seares.2003.05.005.
Hagen, W., Auel, H., 2001. Seasonal adaptations and the role of lipids in oceanic zooplankton. Zoology 104, 313–326. https://doi.org/10.1078/0944-2006-00037.
Hamm, C.E., Merkel, R., Springer, O., Jurkojc, P., Maiert, C., Prechtelt, K., et al., 2003. Architecture and material properties of diatom shells provide effective mechanical protection. Nature 421, 841–843. https://doi.org/10.1038/nature01416.
Hicks, Y.A., Marshall, D., Rosin, P.L., Martin, R.R., Mann, D.G., Droop, S.J.M, 2006. A model of diatom shape and texture for analysis, synthesis and identification. Mach. Vis. Appl. 17, 297–307. https://doi.org/10.1007/s00138-006-0035-1.
Hildebrand, M., Frigeri, L.G., Davis, A.K., 2007. Synchronized growth of *Thalassiosira pseudonana* (Bacillariophyceae) provides novel insights into cell-wall synthesis processes in relation to the cell cycle. J. Phycol. 43, 730–740. https://doi.org/10.1111/j.1529-8817.2007.00361.x.
Hoppenrath, M., Beszteri, B., Drebes, G., Halliger, H., Van Beusekom, J.E.E., Janisch, S., et al., 2007. *Thalassiosira* species (Bacillariophyceae, Thalassiosirales) in the North Sea at Helgoland (German Bight) and Sylt (North Frisian Wadden Sea) - A first approach to assessing diversity. Eur. J. Phycol. 42, 271–288. https://doi.org/10.1080/09670260701352288.
Ingólfsson, H.I., Lopez, C.A., Uusitalo, J.J., de Jong, D.H., Gopal, S.M., Periole, X., et al., 2014. The power of coarse graining in biomolecular simulations. Wiley Interdiscip. Rev. Comput. Mol. Sci. 4, 225–248. https://doi.org/10.1002/wcms.1169.
Inomura, K., Masuda, T., Gauglitz, J.M., 2019. Active nitrogen fixation by *Crocosphaera* expands their niche despite the presence of ammonium – a case study. Nat. Sci. Rep. 9, 1–11. https://doi.org/10.1038/s41598-019-51378-4.
Inomura, K., Omta, A.W., Talmy, D., Bragg, J., Deutsch, C., Follows, M.J., 2020. A mechanistic model of macromolecular allocation, elemental stoichiometry, and growth rate in phytoplankton. Front. Microbiol. 11, 1–22. https://doi.org/10.3389/fmicb.2020.00086.
Jahn, M., Vialas, V., Karlsen, J., Maddalo, G., Edfors, F., Forsström, B., et al., 2018. Growth of cyanobacteria is constrained by the abundance of light and carbon assimilation proteins. Cell Rep. 25, 478–486. https://doi.org/10.1016/j.celrep.2018.09.040 e8.
King, A.L., Jenkins, B.D., Wallace, J.R., Liu, Y., Wikfors, G.H., Milke, L.M., et al., 2015. Effects of CO_2 on growth rate, C:N:P, and fatty acid composition of seven marine phytoplankton species. Mar. Ecol. Prog. Ser. 537, 59–69. https://doi.org/10.3354/meps11458.
Kipp, R. M., McCarthy, M., and Fusaro, A. (2019). *Thalassiosira pseudonana* (Hustedt) Hasle and Heimdal (1957) 1970. U.S. Geol. Surv. Nonindigenous Aquat. Species Database, Gainesville, FL, NOAA Gt. Lakes Aquat. Nonindigenous Species Inf. Syst. Ann Arbor, MI. Available at: https://nas.er.usgs.gov/queries/GreatLakes/FactSheet.aspx?Species_ID=1692.
Kmiecik, S., Gront, D., Kolinski, M., Wieteska, L., Dawid, A.E., Kolinski, A., 2016. Coarse-grained protein models and their applications. Chem. Rev. 116, 7898–7936. https://doi.org/10.1021/acs.chemrev.6b00163.
Kranzler, C.F., Krause, J.W., Brzezinski, M.A., Edwards, B.R., Biggs, W.P., Maniscalco, M., et al., 2019. Silicon limitation facilitates virus infection and mortality of marine diatoms. Nat. Microbiol. 1790–1797.
Leblanc, K., Arístegui, J., Armand, L., Assmy, P., Beker, B., Bode, A., et al., 2012. A global diatom database- a bundance, biovolume and biomass in the world ocean. Earth Syst. Sci. Data 4, 149–165. https://doi.org/10.5194/essd-4-149-2012.
Legendre, L., Le Fevre, J, 1995. Microbial food webs and the export of biogenic carbon in oceans. Aquat. Microb. Ecol. 9, 69–77. https://doi.org/10.3354/ame009069.
Lomas, M.W., Glibert, P.M., 2000. Comparisons of nitrate uptake, storage, and reduction in marine diatoms and flagellates. J. Phycol. 913, 903–913.
Lu, J., Sun, C., Wang, Q.J., 2015. Mechanical simulation of a diatom frustule structure. J. Bionic Eng. 12, 98–108. https://doi.org/10.1016/S1672-6529(14)60104-9.
Lynn, S.G., Kilham, S.S., Kreeger, D.A., Interlandi, S.J., 2000. Effect of nutrient availability on the biochemical and elemental stoichiometry in the freshwater diatom *Stephanodiscus minutulus* (Bacillariophyceae). J. Phycol. 36, 510–522. https://doi.org/10.1046/j.1529-8817.2000.98251.x.
Makareviciute-Fichtner, K., Matthiessen, B., Lotze, H.K., Sommer, U., 2021. Phytoplankton nutritional quality is altered by shifting Si:N ratios and selective grazing. J. Plankton Res. 43, 325–337. https://doi.org/10.1093/plankt/fbab034.
Martin-Jézéquel, V., Hildebrand, M., Brzezinski, M.A., 2000. Silicon metabolism in diatoms: implications for growth. J. Phycol. 36, 821–840. https://doi.org/10.1046/j.1529-8817.2000.00019.x.
Michaels, A.F., Silver, M.W., 1988. Primary production, sinking fluxes, and the microbial food web. Deep. Res. 35, 473–490.
Nicklisch, A., Steinberg, C.E.W., 2009. RNA/protein and RNA/DNA ratios determined by flow cytometry and their relationship to growth limitation of selected planktonic algae in culture. Eur. J. Phycol. 44, 297–308. https://doi.org/10.1080/09670260802578518.
Obata, T., Fernie, A.R., Nunes-Nesi, A., 2013. The central carbon and energy metabolism of marine diatoms. Metabolites 3, 325–346. https://doi.org/10.3390/metabo3020325.
Paasche, E., 1973. Silicon and the ecology of marine plankton diatoms. II. Silicate-uptake kinetics in five diatom species. Mar. Biol. 19, 262–269. https://doi.org/10.1007/BF02097147.
Panagiotopoulos, C., Goutx, M., Suroy, M., Moriceau, B., 2020. Phosphorus limitation affects the molecular composition of *Thalassiosira weissflogii* leading to increased biogenic silica dissolution and high degradation rates of cellular carbohydrates. Org. Geochem. 148, 104068 https://doi.org/10.1016/j.orggeochem.2020.104068.
Parker, M.S., Mock, T., Armbrust, E.V., 2008. Genomic insights into marine microalgae. Annu. Rev. Genet. 42, 619–645. https://doi.org/10.1146/annurev.genet.42.110807.091417.
Pratt, D.M., 1965. The winter-spring diatom flowering in Narragansett Bay. Limnol. Oceanogr. 10, 173–184.
Quigg, A., Finkel, Z.V., Irwin, A.J., Rosenthal, Y., Ho, T.-Y., Reinfelder, J.R., et al., 2003. Evolutionary inheritance of elemental stoichiometry in phytoplankton. Nature 425, 291–294. https://doi.org/10.1038/nature01953.
Raven, J.A., 1997. The vacuole:a cost-benefit analysis. Adv. Bot. Res. 25, 59–86.
Rhee, G.-Y., 1978. Effects of N : p atomic ratios and nitrate limitation on algal growth, cell composition, and nitrate uptake. Limnol. Oceanogr. 23, 10–25. https://doi.org/10.4319/lo.1978.23.1.0010.
Richardson, T.L., Jackson, G.A, 2007. Small phytoplankton and carbon export from the surface ocean. Science 315, 838–840.
Ruess, L., Müller-Navarra, D.C., 2019. Essential biomolecules in food webs. Front. Ecol. Evol. 7, 1–18. https://doi.org/10.3389/fevo.2019.00269.
Rynearson, T.A., Flickinger, S.A., Fontaine, D.N., 2020. Metabarcoding reveals temporal patterns of community composition and realized thermal niches of *Thalassiosira spp.* (bacillariophyceae) from the narragansett bay long-term plankton time series. Biology 9. https://doi.org/10.3390/biology9010019 (Basel).
Scott, M., Gunderson, C.W., Mateescu, E.M., Zhang, Z., Hwa, T, 2010. Interdependence of cell growth and gene expression: origins and consequences. Science 330, 1099–1102.
Sen, D., Garcia, A.P., Buehler, M.J., 2011. Mechanics of nano-honeycomb silica structures: size-dependent brittle-to-ductile transition. J. Nanomech. Micromech. 1, 112–118. https://doi.org/10.1061/(asce)nm.2153-5477.0000037.
Smetacek, V.S., 1985. Role of sinking in diatom life-history cycles: ecological, evolutionary and geological significance. Mar. Biol. 84, 239–251. https://doi.org/10.1007/BF00392493.
Smith, R.E.H., Geider, R.J., 1985. Kinetics of intracellular carbon allocation in a marine diatom. J. Exp. Mar. Bio. Ecol. 93, 191–210. https://doi.org/10.1016/0022-0981(85)90239-4.
Spilling, K., Ylöstalo, P., Simis, S., Seppälä, J., 2015. Interaction effects of light, temperature and nutrient limitations (N, P and Si) on growth, stoichiometry and photosynthetic parameters of the cold-water diatom *Chaetoceros wighamii*. PLoS One 10, 1–18. https://doi.org/10.1371/journal.pone.0126308.
Strohm, T.O., Griffin, B., Zumft, W.G., Schink, B., 2007. Growth yields in bacterial denitrification and nitrate ammonification. Appl. Environ. Microbiol. 73, 1420–1424. https://doi.org/10.1128/AEM.02508-06.
Thamatrakoln, K., Hildebrand, M., 2008. Silicon uptake in diatoms revisited: a model for saturable and nonsaturable uptake kinetics and the role of silicon transporters. Plant Physiol. 146, 1397–1407. https://doi.org/10.1104/pp.107.107094.
Thauer, R.K., Jungermann, K., Decker, K., 1977. Energy conservation in chemotrophic anaerobic bacteria. Bacteriol. Rev. 41, 100–180. https://doi.org/10.1108/eb027807.
Tilman, D., Kilham, S.S., 1976. Phosphate and Silicate growth and uptake kinetics of the diatoms *Asterionella formosa* and cyclotella meneghiniana in batch and continuous culture. J. Phycol. 12, 375–383.
Topal, E., Rajendran, H., Zgłobicka, I., Gluch, J., Liao, Z., Clausner, A., et al., 2020. Numerical and experimental study of the mechanical response of diatom frustules. Nanomaterials 10, 1–14. https://doi.org/10.3390/nano10050959.
Tozzi, S., Schofield, O., Falkowski, P., 2004. Historical climate change and ocean turbulence as selective agents for two key phytoplankton functional groups. Mar. Ecol. Prog. Ser. 274, 123–132. https://doi.org/10.3354/meps274123.
Tréguer, P., Bowler, C., Moriceau, B., Dutkiewicz, S., Gehlen, M., Aumont, O., et al., 2018. Influence of diatom diversity on the ocean biological carbon pump. Nat. Geosci. 11, 27–37. https://doi.org/10.1038/s41561-017-0028-x.
Waite, A., Fisher, A., Thompson, P.A., Harrison, P.J., 1997. Sinking rate versus cell volume relationships illuminate sinking rate control mechanisms in marine diatoms. Mar. Ecol. Prog. Ser. 157, 97–108. https://doi.org/10.3354/meps157097.
Waite, A.M., Thompson, P.A., Harrison, P.J., 1992. Does energy control the sinking rates of marine diatoms? Limnol. Oceanogr. 37, 468–477. https://doi.org/10.4319/lo.1992.37.3.0468.
Watanabe, S., Hajima, T., Sudo, K., Nagashima, T., Takemura, T., Okajima, H., et al., 2011. MIROC-ESM 2010: model description and basic results of CMIP5-20c3m experiments. Geosci. Model Dev. 4, 845–872. https://doi.org/10.5194/gmd-4-845-2011.
Wheeler, P.A., 1983. Phytoplankton nitrogen metabolism. Nitrogen in the Marine Environment. (Academic Press), pp. 309–346. https://doi.org/10.1016/B978-0-12-160280-2.50017-1.

Yoshie, N., Suzuki, K., Kuwata, A., Nishioka, J., Saito, H., 2010. Temporal and spatial variations in photosynthetic physiology of diatoms during the spring bloom in the western subarctic Pacific. Mar. Ecol. Prog. Ser. 399, 39–52. https://doi.org/10.3354/meps08329.

Yvon-Durocher, G., Dossena, M., Trimmer, M., Woodward, G., Allen, A.P, 2015. Temperature and the biogeography of algal stoichiometry. Glob. Ecol. Biogeogr. 24, 562–570. https://doi.org/10.1111/geb.12280.

Zahariev, K., Christian, J.R., Denman, K.L., 2008. Preindustrial, historical, and fertilization simulations using a global ocean carbon model with new parameterizations of iron limitation, calcification, and N2 fixation. Prog. Oceanogr. 77, 56–82. https://doi.org/10.1016/j.pocean.2008.01.007.

Zavřel, T., Faizi, M., Loureiro, C., Poschmann, G., Stühler, K., Sinetova, M., et al., 2019. Quantitative insights into the cyanobacterial cell economy. Elife 8, 1–29. https://doi.org/10.7554/eLife.42508.

Van Tol, H. M., and Virginia Armbrust, E. (2021). Genome-scale metabolic model of the diatom *Thalassiosira pseudonana* highlights the importance of nitrogen and sulfur metabolism in redox balance. doi:10.1371/journal.pone.0241960.